

Study of the Suppressed Decays $B^\pm \rightarrow [K^\mp \pi^\pm]_D K^\pm$ and $B^\pm \rightarrow [K^\mp \pi^\pm]_D \pi^\pm$ at Belle

K. Abe,⁹ K. Abe,⁴⁷ I. Adachi,⁹ H. Aihara,⁴⁹ K. Aoki,²³ K. Arinstein,² Y. Asano,⁵⁴
T. Aso,⁵³ V. Aulchenko,² T. Aushev,¹³ T. Aziz,⁴⁵ S. Bahinipati,⁵ A. M. Bakich,⁴⁴
V. Balagura,¹³ Y. Ban,³⁶ S. Banerjee,⁴⁵ E. Barberio,²² M. Barbero,⁸ A. Bay,¹⁹ I. Bedny,²
U. Bitenc,¹⁴ I. Bizjak,¹⁴ S. Blyth,²⁵ A. Bondar,² A. Bozek,²⁹ M. Bračko,^{9, 21, 14}
J. Brodzicka,²⁹ T. E. Browder,⁸ M.-C. Chang,⁴⁸ P. Chang,²⁸ Y. Chao,²⁸ A. Chen,²⁵
K.-F. Chen,²⁸ W. T. Chen,²⁵ B. G. Cheon,⁴ C.-C. Chiang,²⁸ R. Chistov,¹³ S.-K. Choi,⁷
Y. Choi,⁴³ Y. K. Choi,⁴³ A. Chuvikov,³⁷ S. Cole,⁴⁴ J. Dalseno,²² M. Danilov,¹³ M. Dash,⁵⁶
L. Y. Dong,¹¹ R. Dowd,²² J. Dragic,⁹ A. Drutskoy,⁵ S. Eidelman,² Y. Enari,²³
D. Epifanov,² F. Fang,⁸ S. Fratina,¹⁴ H. Fujii,⁹ N. Gabyshev,² A. Garmash,³⁷
T. Gershon,⁹ A. Go,²⁵ G. Gokhroo,⁴⁵ P. Goldenzweig,⁵ B. Golob,^{20, 14} A. Gorišek,¹⁴
M. Grosse Perdekamp,³⁸ H. Guler,⁸ R. Guo,²⁶ J. Haba,⁹ K. Hara,⁹ T. Hara,³⁴
Y. Hasegawa,⁴² N. C. Hastings,⁴⁹ K. Hasuko,³⁸ K. Hayasaka,²³ H. Hayashii,²⁴ M. Hazumi,⁹
T. Higuchi,⁹ L. Hinz,¹⁹ T. Hojo,³⁴ T. Hokuue,²³ Y. Hoshi,⁴⁷ K. Hoshina,⁵² S. Hou,²⁵
W.-S. Hou,²⁸ Y. B. Hsiung,²⁸ Y. Igarashi,⁹ T. Iijima,²³ K. Ikado,²³ A. Imoto,²⁴ K. Inami,²³
A. Ishikawa,⁹ H. Ishino,⁵⁰ K. Itoh,⁴⁹ R. Itoh,⁹ M. Iwasaki,⁴⁹ Y. Iwasaki,⁹ C. Jacoby,¹⁹
C.-M. Jen,²⁸ R. Kagan,¹³ H. Kakuno,⁴⁹ J. H. Kang,⁵⁷ J. S. Kang,¹⁶ P. Kapusta,²⁹
S. U. Kataoka,²⁴ N. Katayama,⁹ H. Kawai,³ N. Kawamura,¹ T. Kawasaki,³¹ S. Kazi,⁵
N. Kent,⁸ H. R. Khan,⁵⁰ A. Kibayashi,⁵⁰ H. Kichimi,⁹ N. Kikichi,⁴⁸ H. J. Kim,¹⁸
H. O. Kim,⁴³ J. H. Kim,⁴³ S. K. Kim,⁴¹ S. M. Kim,⁴³ T. H. Kim,⁵⁷ K. Kinoshita,⁵
N. Kishimoto,²³ S. Korpar,^{21, 14} Y. Kozakai,²³ P. Križan,^{20, 14} P. Krokovny,⁹ T. Kubota,²³
R. Kulasiri,⁵ C. C. Kuo,²⁵ H. Kurashiro,⁵⁰ E. Kurihara,³ A. Kusaka,⁴⁹ A. Kuzmin,²
Y.-J. Kwon,⁵⁷ J. S. Lange,⁶ G. Leder,¹² S. E. Lee,⁴¹ Y.-J. Lee,²⁸ T. Lesiak,²⁹ J. Li,⁴⁰
A. Limosani,⁹ S.-W. Lin,²⁸ D. Liventsev,¹³ J. MacNaughton,¹² G. Majumder,⁴⁵ F. Mandl,¹²
D. Marlow,³⁷ H. Matsumoto,³¹ T. Matsumoto,⁵¹ A. Matyja,²⁹ Y. Mikami,⁴⁸ W. Mitaroff,¹²
K. Miyabayashi,²⁴ H. Miyake,³⁴ H. Miyata,³¹ Y. Miyazaki,²³ R. Mizuk,¹³ D. Mohapatra,⁵⁶
G. R. Moloney,²² T. Mori,⁵⁰ A. Murakami,³⁹ T. Nagamine,⁴⁸ Y. Nagasaka,¹⁰
T. Nakagawa,⁵¹ I. Nakamura,⁹ E. Nakano,³³ M. Nakao,⁹ H. Nakazawa,⁹ Z. Natkaniec,²⁹
K. Neichi,⁴⁷ S. Nishida,⁹ O. Nitoh,⁵² S. Noguchi,²⁴ T. Nozaki,⁹ A. Ogawa,³⁸ S. Ogawa,⁴⁶
T. Ohshima,²³ T. Okabe,²³ S. Okuno,¹⁵ S. L. Olsen,⁸ Y. Onuki,³¹ W. Ostrowicz,²⁹
H. Ozaki,⁹ P. Pakhlov,¹³ H. Palka,²⁹ C. W. Park,⁴³ H. Park,¹⁸ K. S. Park,⁴³ N. Parslow,⁴⁴
L. S. Peak,⁴⁴ M. Pernicka,¹² R. Pestotnik,¹⁴ M. Peters,⁸ L. E. Piilonen,⁵⁶ A. Poluektov,²
F. J. Ronga,⁹ N. Root,² M. Rozanska,²⁹ H. Sahoo,⁸ M. Saigo,⁴⁸ S. Saitoh,⁹ Y. Sakai,⁹
H. Sakamoto,¹⁷ H. Sakaue,³³ T. R. Sarangi,⁹ M. Satapathy,⁵⁵ N. Sato,²³ N. Satoyama,⁴²
T. Schietinger,¹⁹ O. Schneider,¹⁹ P. Schönmeier,⁴⁸ J. Schümann,²⁸ C. Schwanda,¹²
A. J. Schwartz,⁵ T. Seki,⁵¹ K. Senyo,²³ R. Seuster,⁸ M. E. Sevier,²² T. Shibata,³¹
H. Shibuya,⁴⁶ J.-G. Shiu,²⁸ B. Shwartz,² V. Sidorov,² J. B. Singh,³⁵ A. Somov,⁵ N. Soni,³⁵
R. Stamen,⁹ S. Stanič,³² M. Starič,¹⁴ A. Sugiyama,³⁹ K. Sumisawa,⁹ T. Sumiyoshi,⁵¹
S. Suzuki,³⁹ S. Y. Suzuki,⁹ O. Tajima,⁹ N. Takada,⁴² F. Takasaki,⁹ K. Tamai,⁹ N. Tamura,³¹
K. Tanabe,⁴⁹ M. Tanaka,⁹ G. N. Taylor,²² Y. Teramoto,³³ X. C. Tian,³⁶ K. Trabelsi,⁸

Y. F. Tse,²² T. Tsuboyama,⁹ T. Tsukamoto,⁹ K. Uchida,⁸ Y. Uchida,⁹ S. Uehara,⁹
T. Uglov,¹³ K. Ueno,²⁸ Y. Unno,⁹ S. Uno,⁹ P. Urquijo,²² Y. Ushiroda,⁹ G. Varner,⁸
K. E. Varvell,⁴⁴ S. Villa,¹⁹ C. C. Wang,²⁸ C. H. Wang,²⁷ M.-Z. Wang,²⁸ M. Watanabe,³¹
Y. Watanabe,⁵⁰ L. Widhalm,¹² C.-H. Wu,²⁸ Q. L. Xie,¹¹ B. D. Yabsley,⁵⁶ A. Yamaguchi,⁴⁸
H. Yamamoto,⁴⁸ S. Yamamoto,⁵¹ Y. Yamashita,³⁰ M. Yamauchi,⁹ Heyoung Yang,⁴¹
J. Ying,³⁶ S. Yoshino,²³ Y. Yuan,¹¹ Y. Yusa,⁴⁸ H. Yuta,¹ S. L. Zang,¹¹ C. C. Zhang,¹¹
J. Zhang,⁹ L. M. Zhang,⁴⁰ Z. P. Zhang,⁴⁰ V. Zhilich,² T. Ziegler,³⁷ and D. Zürcher¹⁹

(The Belle Collaboration)

¹*Aomori University, Aomori*

²*Budker Institute of Nuclear Physics, Novosibirsk*

³*Chiba University, Chiba*

⁴*Chonnam National University, Kwangju*

⁵*University of Cincinnati, Cincinnati, Ohio 45221*

⁶*University of Frankfurt, Frankfurt*

⁷*Gyeongsang National University, Chinju*

⁸*University of Hawaii, Honolulu, Hawaii 96822*

⁹*High Energy Accelerator Research Organization (KEK), Tsukuba*

¹⁰*Hiroshima Institute of Technology, Hiroshima*

¹¹*Institute of High Energy Physics,
Chinese Academy of Sciences, Beijing*

¹²*Institute of High Energy Physics, Vienna*

¹³*Institute for Theoretical and Experimental Physics, Moscow*

¹⁴*J. Stefan Institute, Ljubljana*

¹⁵*Kanagawa University, Yokohama*

¹⁶*Korea University, Seoul*

¹⁷*Kyoto University, Kyoto*

¹⁸*Kyungpook National University, Taegu*

¹⁹*Swiss Federal Institute of Technology of Lausanne, EPFL, Lausanne*

²⁰*University of Ljubljana, Ljubljana*

²¹*University of Maribor, Maribor*

²²*University of Melbourne, Victoria*

²³*Nagoya University, Nagoya*

²⁴*Nara Women's University, Nara*

²⁵*National Central University, Chung-li*

²⁶*National Kaohsiung Normal University, Kaohsiung*

²⁷*National United University, Miao Li*

²⁸*Department of Physics, National Taiwan University, Taipei*

²⁹*H. Niewodniczanski Institute of Nuclear Physics, Krakow*

³⁰*Nippon Dental University, Niigata*

³¹*Niigata University, Niigata*

³²*Nova Gorica Polytechnic, Nova Gorica*

³³*Osaka City University, Osaka*

³⁴*Osaka University, Osaka*

³⁵*Panjab University, Chandigarh*

³⁶*Peking University, Beijing*

³⁷*Princeton University, Princeton, New Jersey 08544*

³⁸*RIKEN BNL Research Center, Upton, New York 11973*

³⁹*Saga University, Saga*

⁴⁰*University of Science and Technology of China, Hefei*

⁴¹*Seoul National University, Seoul*

⁴²*Shinshu University, Nagano*

⁴³*Sungkyunkwan University, Suwon*

⁴⁴*University of Sydney, Sydney NSW*

⁴⁵*Tata Institute of Fundamental Research, Bombay*

⁴⁶*Toho University, Funabashi*

⁴⁷*Tohoku Gakuin University, Tagajo*

⁴⁸*Tohoku University, Sendai*

⁴⁹*Department of Physics, University of Tokyo, Tokyo*

⁵⁰*Tokyo Institute of Technology, Tokyo*

⁵¹*Tokyo Metropolitan University, Tokyo*

⁵²*Tokyo University of Agriculture and Technology, Tokyo*

⁵³*Toyama National College of Maritime Technology, Toyama*

⁵⁴*University of Tsukuba, Tsukuba*

⁵⁵*Utkal University, Bhubaneswer*

⁵⁶*Virginia Polytechnic Institute and State University, Blacksburg, Virginia 24061*

⁵⁷*Yonsei University, Seoul*

Abstract

We report an updated study of the suppressed decays $B^- \rightarrow [K^+\pi^-]_D K^-$ and $B^- \rightarrow [K^+\pi^-]_D \pi^-$ where $[K^+\pi^-]_D$ indicates that the $K^+\pi^-$ pair originates from a neutral D meson. A data sample containing 386 million $B\bar{B}$ pairs recorded at the $\Upsilon(4S)$ resonance with the Belle detector at the KEKB asymmetric e^+e^- storage ring is used. This decay mode is sensitive to the CKM angle ϕ_3 . We do not see a significant signal for $B^- \rightarrow [K^+\pi^-]_D K^-$, and we set a limit on the ratio of B decay amplitudes $r_B < 0.18$ at the 90% confidence level. We measure the CP asymmetry of the $B^- \rightarrow [K^+\pi^-]_D \pi^-$ mode, $\mathcal{A}_{D\pi} = 0.10 \pm 0.22$ (stat) ± 0.02 (syst).

INTRODUCTION

Precise measurements of the elements of the Cabibbo-Kobayashi-Maskawa matrix [1] constrain the Standard Model and may reveal new physics. However, the extraction of the Unitarity Triangle angle ϕ_3 [2] is a challenging measurement even with modern high luminosity B factories. Several methods for measuring ϕ_3 use the interference between $B^- \rightarrow D^0 K^-$ and $B^- \rightarrow \bar{D}^0 K^-$, which occurs when D^0 and \bar{D}^0 decay to common final states [3, 4]. CP violation occurs when both weak and strong phase differences between the amplitudes are non-trivial. As noted by Atwood, Dunietz and Soni (ADS) [5], CP violation effects are enhanced if the final state is chosen so that the interfering amplitudes have comparable magnitudes; the archetype uses $B^- \rightarrow [K^+\pi^-]_D K^-$, where $[K^+\pi^-]_D$ indicates that the $K^+\pi^-$ pair originates from a neutral D meson. In this case, the colour-allowed B decay followed by the doubly Cabibbo-suppressed D decay interferes with the colour-suppressed B decay followed by the Cabibbo-allowed D decay (Fig. 1). Previous studies of this decay mode by BaBar [6] and Belle [7] have not found any significant signals for $B^- \rightarrow [K^+\pi^-]_D K^-$. For the suppressed decay $B^- \rightarrow [K^+\pi^-]_D \pi^-$, both topology and phenomenology are similar to $B^- \rightarrow [K^+\pi^-]_D K^-$; our previous publication reported the first observation of this mode [7].

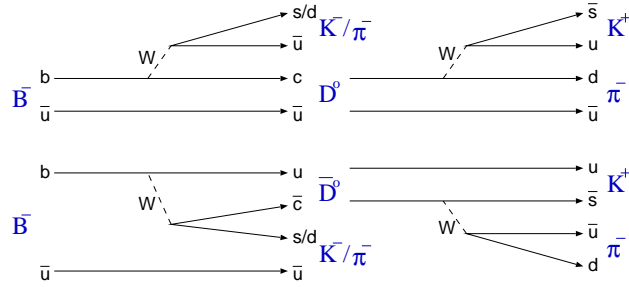


FIG. 1: $B^- \rightarrow [K^+\pi^-]_D K^-$ and $B^- \rightarrow [K^+\pi^-]_D \pi^-$ decays.

ANALYSIS

In this paper, we report an updated analysis of the suppressed decays $B^\pm \rightarrow [K^\mp \pi^\pm]_D K^\pm$ and $B^\pm \rightarrow [K^\mp \pi^\pm]_D \pi^\pm$. In addition, the allowed decays $B^\pm \rightarrow [K^\pm \pi^\mp]_D K^\pm$ and $B^\pm \rightarrow [K^\pm \pi^\mp]_D \pi^\pm$ are used as control samples to reduce systematic uncertainties. The same selection criteria for the suppressed decay modes are applied to the control samples whenever possible. The main changes with respect to our previous publication [7] are the inclusion of additional data corresponding to 111 million $B\bar{B}$ pairs, and improved suppression of the dominant continuum background. Throughout this report, charge conjugate states are implied except where explicitly mentioned and we denote the analysed decay modes as follows:

$$\begin{aligned} \text{Suppressed decay } B^- \rightarrow [K^+\pi^-]_D h^- : \quad & B^- \rightarrow D_{\text{sup}} h^- \\ \text{Allowed decay } B^- \rightarrow [K^-\pi^+]_D h^- : \quad & B^- \rightarrow D_{\text{fav}} h^- \quad (h = K, \pi). \end{aligned}$$

The results are based on a data sample containing 386 million $B\bar{B}$ pairs collected at the $\Upsilon(4S)$ resonance with the Belle detector at the KEKB asymmetric energy e^+e^- collider [8].

The Belle detector is a large-solid-angle magnetic spectrometer that consists of a silicon vertex detector (SVD), a 50-layer central drift chamber (CDC), an array of aerogel threshold Čerenkov counters (ACC), a barrel-like arrangement of time-of-flight scintillation counters (TOF), and an electromagnetic calorimeter (ECL) comprised of CsI(Tl) crystals located inside a superconducting solenoid coil that provides a 1.5 T magnetic field. An iron flux-return located outside of the coil is instrumented to detect K_L^0 mesons and to identify muons (KLM). The detector is described in detail elsewhere [9]. Two different inner detector configurations were used. For the first sample of 152 million $B\bar{B}$ pairs, a 2.0 cm radius beampipe and a 3-layer silicon vertex detector were used; for the latter 234 million $B\bar{B}$ pairs, a 1.5 cm radius beampipe, a 4-layer silicon detector and a small-cell inner drift chamber were used [10].

Event selection

D mesons are reconstructed by combining two oppositely charged tracks. These charged tracks are required to have a point of closest approach to the beam line within ± 5 mm of the interaction point in the direction perpendicular to the beam axis (dr) and ± 5 cm in the direction antiparallel to the positron beam axis (dz). A K/π likelihood ratio $P(K/\pi) = \mathcal{L}_K/(\mathcal{L}_K + \mathcal{L}_\pi)$ is formed for each track, where \mathcal{L}_K and \mathcal{L}_π are kaon and pion likelihoods, calculated using dE/dx measurements from the CDC, Čerenkov light yields in the ACC and timing information from the TOF. We used the particle identification requirement $P(K/\pi) > 0.4$ and $P(K/\pi) < 0.7$ for kaons and pions from $D \rightarrow K\pi$ decays, respectively. D candidates are required to have an invariant mass within $\pm 2.5\sigma$ of the nominal D^0 mass: $1.850 \text{ GeV}/c^2 < M(K\pi) < 1.879 \text{ GeV}/c^2$. To improve the momentum determination, tracks from the D candidate are refitted according to the nominal D^0 mass hypothesis and the reconstructed vertex position (a mass-and-vertex-constrained fit).

B mesons are reconstructed by combining D candidates with primary charged hadron candidates. For the primary charged tracks, we require $P(K/\pi) > 0.6$ for the kaon in $B^- \rightarrow DK^-$ and $P(K/\pi) < 0.2$ for the pion in $B^- \rightarrow D\pi^-$. The signal is identified by two kinematic variables, the energy difference $\Delta E = E_D + E_{K^-(\pi^-)} - E_{\text{beam}}$ and the beam-energy-constrained mass $M_{\text{bc}} = \sqrt{E_{\text{beam}}^2 - (\vec{p}_D + \vec{p}_{K^-(\pi^-)})^2}$, where E_D is the energy of the D candidate, $E_{K^-(\pi^-)}$ is the energy of the $K^-(\pi^-)$ and E_{beam} is the beam energy, in the centre of mass (cm) frame. \vec{p}_D and $\vec{p}_{K^-(\pi^-)}$ are the momenta of the D and $K^-(\pi^-)$ in the cm frame. We define the signal region as $5.27 \text{ GeV}/c^2 < M_{\text{bc}} < 5.29 \text{ GeV}/c^2$ and $-0.05 \text{ GeV} < \Delta E < 0.05 \text{ GeV}$. In the case of multiple candidates, which occurs in 1–2% of events with at least one candidate, we choose the best candidate on the basis of a χ^2 determined from the difference between the measured and nominal values of M_{bc} .

$q\bar{q}$ continuum suppression

To suppress the large background from the two-jet like $e^+e^- \rightarrow q\bar{q}$ ($q = u, d, s, c$) continuum processes, variables that characterise the event topology are used. We construct a Fisher discriminant [11] of modified Fox-Wolfram moments [12], which we denote SFW . The Fisher coefficients are optimized by maximising the separation between signal events and continuum events. Furthermore, $\cos\theta_B$, the angle in the cm system of the B flight direction with respect to the beam axis is also used to distinguish $B\bar{B}$ events from continuum events.

These two independent variables, SFW and $\cos\theta_B$, are combined to form a likelihood ratio (\mathcal{R}),

$$\mathcal{R} = \mathcal{L}_{\text{sig}} / (\mathcal{L}_{\text{sig}} + \mathcal{L}_{\text{cont}})$$

$$\mathcal{L}_{\text{sig(cont)}} = \mathcal{L}_{\text{sig(cont)}}^{SFW} \times \mathcal{L}_{\text{sig(cont)}}^{\cos\theta_B},$$

where \mathcal{L}_{sig} and $\mathcal{L}_{\text{cont}}$ are likelihoods defined from SFW and $\cos\theta_B$ distributions for signal and continuum backgrounds, respectively. We optimize the \mathcal{R} requirement by maximising $S/\sqrt{S+N}$, where S and N denote the expected number of signal and background events in the signal region. The signal expectations are calculated from our previous results [7], the efficiency obtained from Monte Carlo simulation (given later), and the number of $B\bar{B}$ pairs; the background expectations are obtained using events in the M_{bc} sideband ($5.240 \text{ GeV}/c^2 < M_{\text{bc}} < 5.265 \text{ GeV}/c^2$), with the extrapolation into the signal region based on Monte Carlo. For $B^- \rightarrow D_{\text{sup}}K^-(\pi^-)$ we require $\mathcal{R} > 0.90$ (0.74), which retains 40.0% (65.7%) of the signal and removes 99.0% (94.3%) of the continuum background.

Peaking backgrounds

For $B^- \rightarrow D_{\text{sup}}K^-$, one can have a contribution from $B^- \rightarrow D^0\pi^-$, $D^0 \rightarrow K^+K^-$, which has the same final state and can peak under the signal. In order to reject these events, we veto events that satisfy $1.843 \text{ GeV}/c^2 < M(KK) < 1.894 \text{ GeV}/c^2$. The allowed decay $B^- \rightarrow D_{\text{fav}}h^-$ can also cause a peaking background for the suppressed decay modes due to $K\pi$ misidentification. Therefore, we veto events for which the invariant mass of the $K\pi$ pair is inside the D mass cut window when the mass assignments are exchanged. Furthermore, three-body charmless decays $B^- \rightarrow K^+K^-\pi^-$ and $B^- \rightarrow K^+\pi^-\pi^-$ can peak inside the signal region for $B^- \rightarrow D_{\text{sup}}K^-$ and $B^- \rightarrow D_{\text{sup}}\pi^-$, respectively. These peaking backgrounds are estimated from the ΔE distributions of events in a D mass sideband, corresponding to $\pm(2.5-10)\sigma$ away from the nominal D mass ($1.807 \text{ GeV}/c^2 < M(K\pi) < 1.850 \text{ GeV}/c^2$ and $1.879 \text{ GeV}/c^2 < M(K\pi) < 1.937 \text{ GeV}/c^2$). We fit these distributions, which are shown in Fig. 2, using a procedure similar to that used for candidate signal events (described later). For $B^- \rightarrow D_{\text{sup}}\pi^-$, the peaking background estimated by fitting the plot is consistent with zero. Since the Standard Model prediction for the $B^- \rightarrow K^+\pi^-\pi^-$ branching fraction is smaller than 10^{-11} [13], this background contribution is ignored. On the other hand, for $B^- \rightarrow D_{\text{sup}}K^-$, the peaking background yield in the D mass sideband is $7.3^{+6.9}_{-6.0}$ events, from which we expect $2.4^{+2.3}_{-2.0}$ peaking background events inside the ΔE signal region.

After applying all the cuts, the signal efficiencies are 14.6% and 24.5% for $B^- \rightarrow D_{\text{sup}}K^-$ and $B^- \rightarrow D_{\text{sup}}\pi^-$, respectively. The signal yields are extracted by fitting the ΔE distributions.

Fitting the ΔE distributions

Backgrounds from decays such as $B^- \rightarrow D\rho^-$ and $B^- \rightarrow D^*\pi^-$ are distributed in the negative ΔE region and make a small contribution to the signal region. The shape of this $B\bar{B}$ background is modelled as a smoothed histogram from generic Monte Carlo (MC) samples. The continuum background populates the entire ΔE region. We model its shape with as a first order polynomial. The signal ΔE distribution is modelled as the sum of two Gaussian distributions with a common mean.

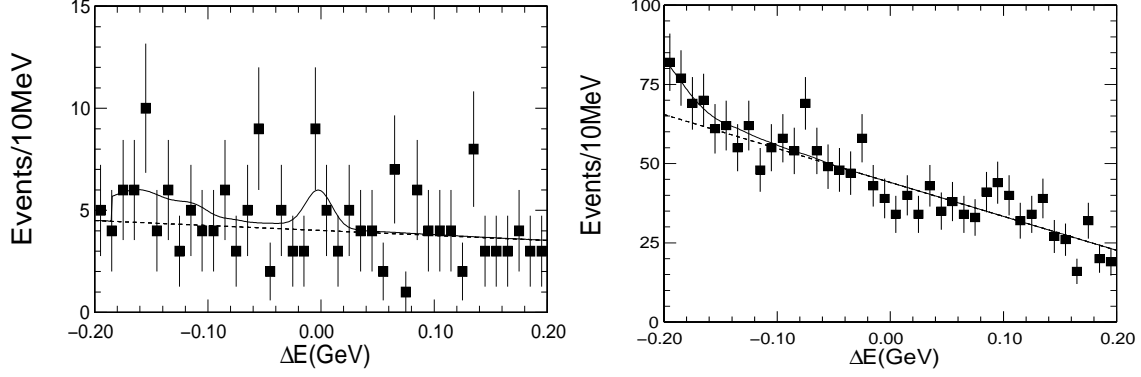


FIG. 2: ΔE distributions for events in the D^0 mass sideband for (left) $B^- \rightarrow D_{\text{sup}} K^-$ and (right) $B^- \rightarrow D_{\text{sup}} \pi^-$. The signal shapes are modelled using the results of the $B^- \rightarrow D_{\text{fav}} h^-$ ($h = K, \pi$) fit.

TABLE I: Efficiencies and signal yields. For the $B^- \rightarrow D_{\text{sup}} K^-$ signal yield, the second value is after subtraction of the peaking background.

Mode	Efficiency (%)	Signal Yield
$B^- \rightarrow D_{\text{sup}} K^-$	14.6 ± 0.2	$2.4^{+4.9}_{-4.4} / 0.0^{+5.3}_{-5.0}$
$B^- \rightarrow D_{\text{sup}} \pi^-$	24.5 ± 0.3	50^{+10}_{-11}
$B^- \rightarrow D_{\text{fav}} K^-$	14.5 ± 0.2	634^{+59}_{-99}
$B^- \rightarrow D_{\text{fav}} \pi^-$	24.9 ± 0.3	14518 ± 125

In the fit to the ΔE distribution of $B^- \rightarrow D_{\text{fav}} \pi^-$, the free parameters are the position, widths, area and fraction in the tail of the signal peak, the slope and normalisation of the continuum component and the normalisation of the $B\bar{B}$ background. For the $B^- \rightarrow D_{\text{fav}} K^-$ fit, there is an additional component due to feed-across from $D_{\text{fav}} \pi^-$, which we model with a Gaussian shape that has different widths on the left and right sides of the peak, since the shift caused by wrong mass assignment makes the shape asymmetric. The normalisation and shape parameters of this function are free parameters of the fit (all parameters which are floated in the $B^- \rightarrow D_{\text{fav}} \pi^-$ fit are again free parameters).

For $B^- \rightarrow D_{\text{sup}} K^-$ and $B^- \rightarrow D_{\text{sup}} \pi^-$, the signal and $B\bar{B}$ background shapes are modelled using the results of the fits to the corresponding favoured modes. The free parameters are the normalisations of the three components, and the slope of the continuum. The amount of feed-across from $D_{\text{sup}} \pi^-$ to $D_{\text{sup}} K^-$ is a free parameter, but is found to be negligible, as expected. The fit results are shown in Fig. 3. The numbers of events for $B^- \rightarrow D_{\text{sup}} h^-$ and $D_{\text{fav}} h^-$ are given in Table I.

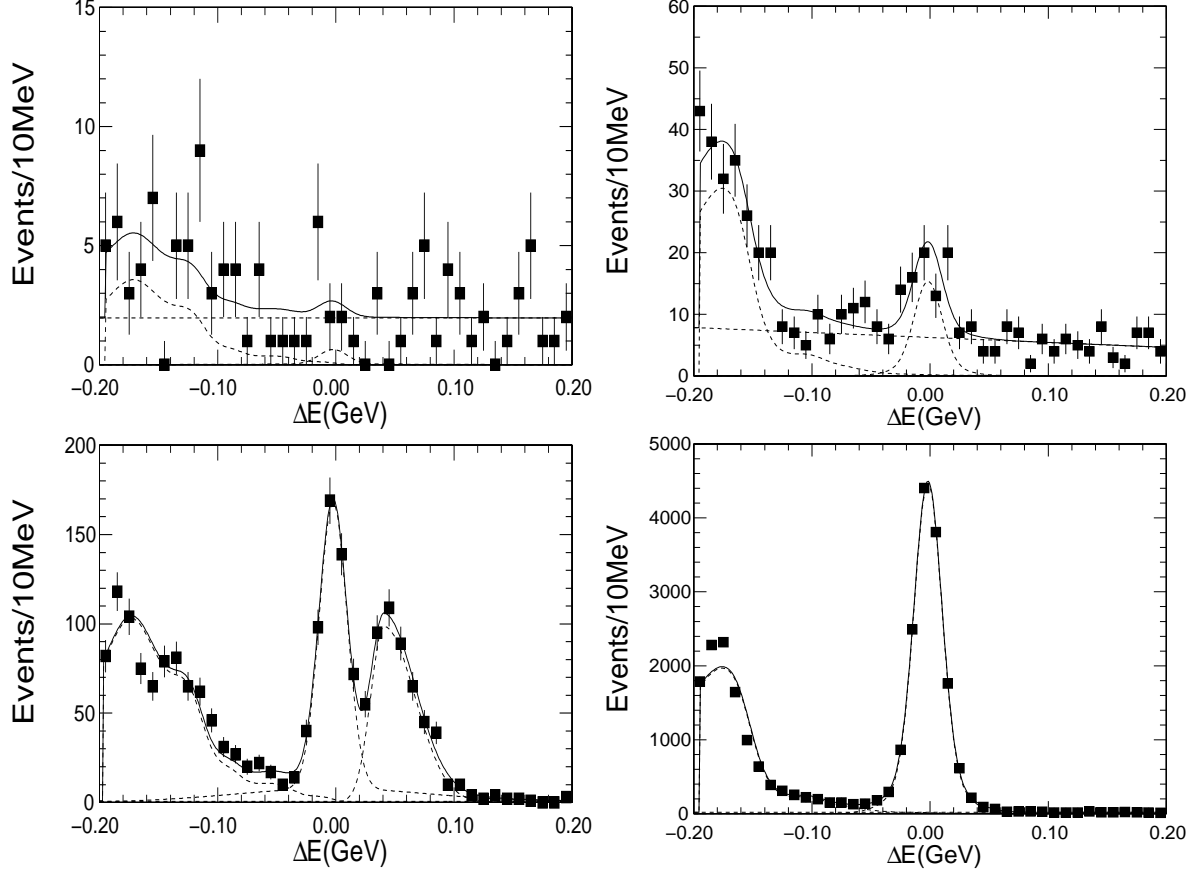


FIG. 3: ΔE fit results for (top left) $B^- \rightarrow D_{\text{sup}} K^-$, (top right) $B^- \rightarrow D_{\text{sup}} \pi^-$, (bottom left) $B^- \rightarrow D_{\text{fav}} K^-$, (bottom right) $B^- \rightarrow D_{\text{fav}} \pi^-$. Charge conjugate modes are included.

RESULTS

Ratio of branching fractions R_{Dh}

We calculate ratios of product branching fractions, defined as

$$R_{Dh} \equiv \frac{\mathcal{B}(B^- \rightarrow D_{\text{sup}} h^-)}{\mathcal{B}(B^- \rightarrow D_{\text{fav}} h^-)} = \frac{N_{D_{\text{sup}} h^-} / \epsilon_{D_{\text{sup}} h^-}}{N_{D_{\text{fav}} h^-} / \epsilon_{D_{\text{fav}} h^-}} \quad (h = K, \pi),$$

where $N_{D_{\text{sup}} h}$ ($N_{D_{\text{fav}} h}$) and $\epsilon_{D_{\text{sup}} h^-}$ ($\epsilon_{D_{\text{fav}} h^-}$) are the number of signal events and the reconstruction efficiency for the decay $B^- \rightarrow D_{\text{sup}} h^-$ ($B^- \rightarrow D_{\text{fav}} h^-$), and are given in Table I. We obtain

$$\begin{aligned} R_{DK} &= (0.0^{+8.4}_{-7.9} (\text{stat}) \pm 1.0 (\text{syst})) \times 10^{-3}, \\ R_{D\pi} &= (3.5^{+0.8}_{-0.7} (\text{stat}) \pm 0.3 (\text{syst})) \times 10^{-3}. \end{aligned}$$

Since the signal for $B^- \rightarrow D_{\text{sup}} K^-$ is not significant, we set an upper limit at the 90% confidence level (C.L.) of $R_{DK} < 13.9 \times 10^{-3}$, where we take the likelihood function as a Gaussian distribution with width given by the quadratic sum of statistical and systematic errors, and the area is normalised in the physical region of positive branching fraction.

Most of the systematic uncertainties from the detection efficiencies and the particle identification cancel when taking the ratios, since the kinematics of the $B^- \rightarrow D_{\text{sup}} h^-$ and $B^- \rightarrow D_{\text{fav}} h^-$ processes are similar. The systematic errors are due to uncertainties in the yield extraction and the efficiency difference between $B^- \rightarrow D_{\text{sup}} h^-$ and $B^- \rightarrow D_{\text{fav}} h^-$. The uncertainties in the signal shapes and the $q\bar{q}$ background shapes are determined by varying the shape of the fitting function by $\pm 1\sigma$. The uncertainties in the $B\bar{B}$ background shapes are determined by fitting the ΔE distribution in the region $-0.07 \text{ GeV} < \Delta E < 0.20 \text{ GeV}$ ignoring the $B\bar{B}$ background contributions — this is the largest source of uncertainty: the signal yields are affected by 7.4% and 28.4% for $D_{\text{sup}}\pi$ and $D_{\text{sup}}K$ (before peaking background subtraction) respectively. The uncertainties in the efficiency differences are determined using signal MC. The total systematic error is the sum in quadrature of the above uncertainties.

The ratio R_{DK} is related to ϕ_3 by

$$R_{DK} = r_B^2 + r_D^2 + 2r_B r_D \cos \phi_3 \cos \delta,$$

where [14]

$$r_B \equiv \left| \frac{A(B^- \rightarrow \bar{D}^0 K^-)}{A(B^- \rightarrow D^0 K^-)} \right|, \quad \delta \equiv \delta_B + \delta_D,$$

$$r_D = \left| \frac{A(D^0 \rightarrow K^+ \pi^-)}{A(D^0 \rightarrow K^- \pi^+)} \right| = 0.060 \pm 0.003.$$

and δ_B (δ_D) is the strong phase difference between the two B (D) decay amplitudes. Using the above result, we obtain a limit on r_B . The least restrictive limit is obtained allowing $\pm 2\sigma$ variation on r_D and assuming maximal interference ($\phi_3 = 0^\circ, \delta = 180^\circ$ or $\phi_3 = 180^\circ, \delta = 0^\circ$) and is found to be $r_B < 0.18$ at the 90% confidence level, as shown in Fig. 4.

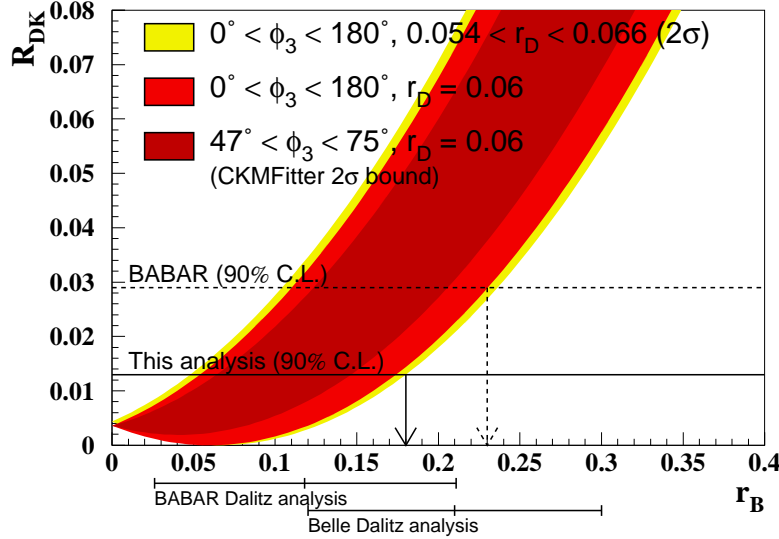


FIG. 4: Constraint on r_B from R_{DK} .

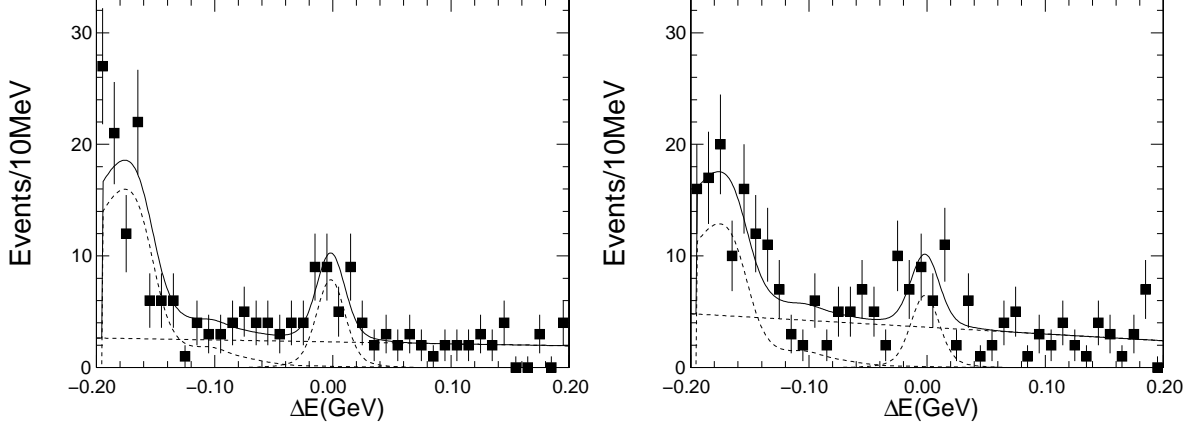


FIG. 5: ΔE fit results for (left) $B^- \rightarrow D_{\text{sup}}\pi^-$ and (right) $B^+ \rightarrow D_{\text{sup}}\pi^+$.

CP asymmetry

We search for CP violating asymmetry in the $B^\pm \rightarrow D_{\text{sup}}\pi^\pm$ mode. We fit the B^+ and B^- yields separately, and determine $\mathcal{A}_{D\pi}$ as

$$\mathcal{A}_{D\pi} \equiv \frac{\mathcal{B}(B^- \rightarrow D_{\text{sup}}\pi^-) - \mathcal{B}(B^+ \rightarrow D_{\text{sup}}\pi^+)}{\mathcal{B}(B^- \rightarrow D_{\text{sup}}\pi^-) + \mathcal{B}(B^+ \rightarrow D_{\text{sup}}\pi^+)}.$$

The fit results are shown in Fig.5. We find $25.6^{+7.4}_{-6.7}$ $B^- \rightarrow D_{\text{sup}}\pi^-$ events and $21.0^{+7.7}_{-7.0}$ $B^+ \rightarrow D_{\text{sup}}\pi^+$ events, giving an asymmetry of

$$\mathcal{A}_{D\pi} = 0.10 \pm 0.22 (\text{stat}) \pm 0.02 (\text{syst}),$$

where systematic uncertainties arise from possible detector charge asymmetry (0.017; determined from the $B^\pm \rightarrow D_{\text{fav}}\pi^\pm$ sample [15]), and the B^+ and B^- yield extraction (0.016; determined as for $R_{D\pi}$). The total systematic error is obtained by taking the quadratic sum. The measured partial rate asymmetry $\mathcal{A}_{D\pi}$ is consistent with zero.

SUMMARY

Using 386 million $B\bar{B}$ pairs collected with the Belle detector, we report studies of the suppressed decays $B^- \rightarrow D_{\text{sup}}h^-$ ($h = K, \pi$). We do not observe a signal for $B^- \rightarrow D_{\text{sup}}K^-$, and place a limit on the ratio of B decay amplitudes $r_B < 0.18$ at the 90% confidence level. We have measured the CP asymmetry in the related mode, $\mathcal{A}_{D\pi} = 0.10 \pm 0.22 (\text{stat}) \pm 0.02 (\text{syst})$.

Acknowledgements

We thank the KEKB group for the excellent operation of the accelerator, the KEK cryogenics group for the efficient operation of the solenoid, and the KEK computer group and the National Institute of Informatics for valuable computing and Super-SINET network

support. We acknowledge support from the Ministry of Education, Culture, Sports, Science, and Technology of Japan and the Japan Society for the Promotion of Science; the Australian Research Council and the Australian Department of Education, Science and Training; the National Science Foundation of China under contract No. 10175071; the Department of Science and Technology of India; the BK21 program of the Ministry of Education of Korea and the CHEP SRC program of the Korea Science and Engineering Foundation; the Polish State Committee for Scientific Research under contract No. 2P03B 01324; the Ministry of Science and Technology of the Russian Federation; the Ministry of Higher Education, Science and Technology of the Republic of Slovenia; the Swiss National Science Foundation; the National Science Council and the Ministry of Education of Taiwan; and the U.S. Department of Energy.

-
- [1] M. Kobayashi and T. Maskawa, *Prog. Theor. Phys.* **49**, 652 (1973).
 - [2] D. Kirkby and Y. Nir, in S. Eidelman *et al.* (Particle Data Group), *Phys. Lett. B* **592**, 1 (2004).
 - [3] I.I. Bigi and A.I. Sanda, *Phys. Lett. B* **211**, 213 (1988).
 - [4] M. Gronau and D. Wyler, *Phys. Lett. B* **165**, 172 (1991); M. Gronau and D. London, *Phys. Lett. B* **253**, 483 (1991).
 - [5] D. Atwood, I. Dunietz, and A. Soni, *Phys. Rev. Lett.* **78**, 3257 (1997); *Phys. Rev. D* **63**, 036005 (2001).
 - [6] B. Aubert *et al.* (BaBar collaboration), hep-ex/0504047, to be submitted to *Phys. Rev. D*.
 - [7] M. Saigo *et al.* (Belle collaboration), *Phys. Rev. Lett.* **94**, 091601 (2005).
 - [8] S. Kurokawa and E. Kikutani, *Nucl. Instr. and Meth. A* **499**, 1 (2003), and other papers included in this volume.
 - [9] A. Abashian *et al.* (Belle collaboration), *Nucl. Instr. and Meth. A* **479**, 117 (2002).
 - [10] Y. Ushiroda (Belle SVD2 Group), *Nucl. Instr. and Meth. A* **511**, 6 (2003).
 - [11] R.A. Fisher, *Ann. Eugenics* **7**, 179 (1936).
 - [12] The Fox-Wolfram moments were introduced in G.C. Fox and S. Wolfram, *Phys. Rev. Lett.* **41**, 1581 (1978). The Fisher discriminant used in this analysis is based on modified Fox-Wolfram moments, and is described in S.H. Lee *et al.* (Belle collaboration), *Phys. Rev. Lett.* **91**, 261801 (2003).
 - [13] K. Huitu, C.D. Lu, P. Singer, D.X. Zhang, *Phys. Rev. Lett.* **81**, 4313 (1998).
 - [14] S. Eidelman *et al.* (Particle Data Group), *Phys. Lett. B* **592**, 1 (2004).
 - [15] In the $B^\pm \rightarrow D_{\text{fav}}\pi^\pm$ sample we measure $\mathcal{A}_{D\pi} = -0.009 \pm 0.008$, from which we estimate a systematic error of ± 0.017 .
 - [16] A. Poluektov *et al.* (Belle collaboration), *Phys. Rev. D* **70**, 072003 (2004).